

# The LisbOn KInetics Monte Carlo solver

## Benchmark calculations

Tiago C Dias, Antonio Tejero-del-Caz, Luís Lemos Alves and Vasco Guerra

email: [loki@tecnico.ulisboa.pt](mailto:loki@tecnico.ulisboa.pt)

September 28, 2022

---

In this document, we present benchmark calculations of the LisbOn KInetics Monte Carlo (LoKI-MC) solver [1] using model gases and real gases. In the case of model gases, the LoKI-MC results are compared with well-established works available in the literature. In real gases, the calculations are compared with the two-term solver LoKI-B [2] and the ten-term solver Multibolt [4].

## Contents

<b>1</b>	<b>Model gases</b>	<b>2</b>
1.1	Reid . . . . .	2
1.2	Lucas-Saelee . . . . .	2
<b>2</b>	<b>Real gases</b>	<b>4</b>
2.1	Ar . . . . .	4
2.2	CF <sub>4</sub> . . . . .	6
2.3	O <sub>2</sub> . . . . .	8
	<b>References</b>	<b>10</b>

# 1 Model gases

For the model gases, we use an ensemble of  $10^5$  electrons. The simulations are stopped when the following requirements for the maximum standard deviations are met: mean energy (0.1%), flux drift velocity (0.4%), flux diffusion coefficients (0.8%) and power balance (0.01%). In all simulations, we used the default values for the numbers of cells used to discretize the distribution functions and for the number of grid points to interpolate the cross sections, defined in [1].

## 1.1 Reid

The Reid model [3] is composed by a constant elastic cross section  $\sigma_c^{\text{el}} = 6 \times 10^{-20} \text{ m}^2$  and a linearly increasing excitation cross section  $\sigma_{\text{exc}} = (\epsilon - 0.2) \times 10^{-19} \text{ m}^2$ , with energy threshold of 0.2 eV. Three values of  $E/N$  are used in this model: 1, 12 and 24 Td. LoKI-MC simulations are compared with MultiBolt [4] and the Monte Carlo results of Raspopović *et al* [5] and White *et al* [6], as shown in table 1. There is an excellent agreement with the results obtained by other codes, for all parameters.

		$\langle \epsilon \rangle$ (eV)	$v_d^b (10^4 \text{ m s}^{-1})$	$D_T^b N (10^{24} \text{ m}^{-1} \text{ s}^{-1})$	$D_L^b N (10^{24} \text{ m}^{-1} \text{ s}^{-1})$
$E/N = 1 \text{ Td}$	LoKI-MC	0.1014 [0.06]	1.264 [0.43]	0.9637 [0.70]	0.7542 [0.68]
	MultiBolt [4]	0.1014 (0.00)	1.272 (-0.63)	0.9746 (-1.13)	0.7593 (-0.68)
	MCC [5]	0.1017 (-0.30)	1.273 (-0.71)	0.966 (-0.24)	0.7575 (-0.44)
	MCC [6]	0.1015 (-0.10)	1.271 (-0.55)	0.974 (-1.07)	0.757 (-0.37)
$E/N = 12 \text{ Td}$	LoKI-MC	0.2691 [0.10]	6.838 [0.09]	1.137 [0.44]	0.5679 [0.35]
	MultiBolt [4]	0.2688 (0.11)	6.839 (-0.01)	1.134 (0.26)	0.5688 (-0.16)
	MCC [5]	0.2703 (-0.45)	6.834 (0.06)	1.140 (-0.26)	0.569 (-2.41)
	MCC [6]	0.2693 (-0.07)	6.833 (0.07)	1.136 (0.09)	0.5816 (-2.41)
$E/N = 24 \text{ Td}$	LoKI-MC	0.4081 [0.10]	8.881 [0.07]	1.138 [0.53]	0.4595 [0.56]
	MultiBolt [4]	0.40922 (-0.27)	8.8522 (0.32)	1.137 (0.09)	0.4601 (-0.13)
	MCC [5]	0.4113 (-0.78)	8.804 (0.87)	1.131 (0.62)	0.4546 (1.07)
	MCC [6]	0.4085 (-0.10)	8.878 (0.03)	1.140 (-0.18)	0.4684 (-1.94)

Table 1: Comparison of LoKI-MC solutions with MultiBolt calculations [4] and previous MC results [5, 6], for the Reid-ramp model [3]. The standard deviations  $\sigma[\%]$  of the LoKI-MC simulations are shown in squared parenthesis. The deviations  $\delta$  between LoKI-MC results (LMC) and previous results (PR), defined as  $\delta[\%] = (1 - \text{PR}/\text{LMC}) \times 100$ , are shown in curved parenthesis.

## 1.2 Lucas-Saelee

We employ the non-conservative model gas of Lucas-Saelee [7], together with the attachment modifications of Ness and Robson [8]:

$$\begin{cases} \sigma_c^{\text{el}} = 4\epsilon^{-1/2} \times 10^{-20} \text{ m}^2 \\ \sigma_{\text{exc}} = 0.1(1 - F)(\epsilon - 15.6) \times 10^{-20} \text{ m}^2 \\ \sigma_{\text{ion}} = 0.1F(\epsilon - 15.6) \times 10^{-20} \text{ m}^2 \\ \sigma_{\text{att}} = a\epsilon^p \times 10^{-20} \text{ m}^2 \end{cases}. \quad (1)$$

The parameter  $F$  controls the fraction of inelastic excitation and ionization. For  $F = 1$ , the excitation cross section,  $\sigma_{\text{exc}}$ , is zero, and for  $F = 0$ , the ionization cross section,  $\sigma_{\text{ion}}$ , is zero. The attachment cross section,  $\sigma_{\text{att}}$ , scales with  $a$  and  $p$  determines the proportionality of the cross section. Different sets of  $\{F, a, p\}$  are used to test the code, including cases of strong ionization or attachment. For all simulations with this model,  $E/N$  is fixed to 10 Td, the gas density is  $N = 10^{20} \text{ m}^{-3}$  and the heavy-particle mass is  $M = 1000 m_e$ . The LoKI-MC calculations are compared with MultiBolt [4] and the MC results of Raspopović [5] and Nolan *et al* [9], as shown in table 2. The general agreement is good, exhibiting differences within two standard deviations.

		$\langle\epsilon\rangle$ (eV)	$\nu_{\text{eff}}$ ( $10^3 \text{ s}^{-1}$ )	$v_d^f$ ( $10^4 \text{ m s}^{-1}$ )	$v_d^b$ ( $10^4 \text{ m s}^{-1}$ )	$D_T^f N$ ( $10^{25} \text{ m}^{-1} \text{ s}^{-1}$ )	$D_T^b N$ ( $10^{25} \text{ m}^{-1} \text{ s}^{-1}$ )	$D_L^f N$ ( $10^{25} \text{ m}^{-1} \text{ s}^{-1}$ )	$D_L^b N$ ( $10^{25} \text{ m}^{-1} \text{ s}^{-1}$ )
$F = 0$ $a = 0$ $p = 0$	LoKI - MC	5.56 [0.05]	0	7.33 [0.40]	7.33 [0.53]	2.73 [0.59]	2.73 [0.78]	2.66 [0.57]	2.68 [0.86]
	MultiBolt [4]	5.56 (0.00)	0 (0.00)	7.33 (0.00)	7.33 (0.00)	2.72 (0.37)	N/A	2.65 (0.38)	2.65 (1.12)
	MCC [9]	5.57 (-0.18)	0 (0.00)	7.32 (0.14)	7.32 (0.14)	2.72 (0.37)	2.72 (0.37)	2.66 (0.00)	2.66 (0.75)
	MCC [5]	5.57 (-0.18)	0 (0.00)	7.28 (0.68)	7.32 (0.14)	2.71 (0.73)	2.73 (0.00)	2.65 (0.38)	2.64 (1.49)
$F = 0.5$ $a = 0$ $p = 0$	LoKI - MC	5.22 [0.05]	1.31	7.28 [0.40]	8.50 [0.52]	2.54 [0.58]	2.70 [1.35]	2.48 [0.62]	2.85 [1.18]
	MultiBolt [4]	5.22 (0.00)	1.33 (-1.53)	7.33 (-0.69)	8.59 (-1.06)	2.55 (-0.39)	N/A	2.50 (-0.81)	2.86 (-0.35)
	MCC [9]	5.22 (0.00)	1.33 (-1.53)	7.32 (-0.55)	8.58 (-0.94)	2.55 (-0.39)	2.73 (-1.11)	2.49 (-0.40)	2.85 (0.00)
	MCC [5]	5.22 (0.00)	1.33 (-1.53)	7.31 (-0.41)	8.58 (-0.94)	2.56 (-0.79)	2.73 (-1.11)	2.49 (-0.40)	2.85 (0.00)
$F = 1.0$ $a = 0$ $p = 0$	LoKI - MC	4.97 [0.05]	2.43	7.36 [0.40]	9.47 [0.53]	2.44 [0.60]	2.75 [1.99]	2.38 [0.62]	2.89 [1.38]
	MultiBolt [4]	4.97 (0.00)	2.42 (0.41)	7.34 (0.27)	9.49 (-0.21)	2.43 (0.41)	N/A	2.38 (0.00)	2.93 (-1.38)
	MCC [9]	4.97 (0.00)	2.42 (0.41)	7.32 (0.54)	9.47 (0.00)	2.43 (0.41)	2.72 (1.09)	2.38 (0.00)	2.94 (-1.73)
	MCC [5]	4.97 (0.00)	2.42 (0.41)	7.30 (0.82)	9.51 (-0.42)	2.42 (0.82)	2.72 (1.09)	2.37 (0.42)	2.93 (-1.38)
$F = 0$ $a = 5 \times 10^{-4}$ $p = 0.5$	LoKI - MC	5.44 [0.06]	-1.61	7.35 [0.40]	7.04 [0.68]	2.67 [0.59]	2.61 [1.56]	2.62 [0.59]	2.74 [1.53]
	MultiBolt [4]	5.43 (0.18)	-1.60 (0.62)	7.33 (0.27)	7.03 (0.14)	2.67 (0.00)	N/A	2.59 (1.15)	2.63 (4.01)
	MCC [9]	5.44 (0.00)	-1.62 (-0.62)	7.33 (0.27)	7.02 (0.28)	2.67 (0.00)	2.61 (0.00)	2.61 (0.38)	2.64 (3.65)
	MCC [5]	5.45 (-0.18)	-1.60 (0.62)	7.30 (0.68)	7.01 (0.43)	2.67 (0.00)	2.63 (-0.77)	2.60 (0.76)	2.66 (2.92)
$F = 0$ $a = 2 \times 10^{-3}$ $p = -0.5$	LoKI - MC	5.55 [0.05]	-1.19	7.34 [0.40]	7.31 [0.47]	2.71 [0.59]	2.77 [1.40]	2.65 [0.60]	2.67 [1.39]
	MultiBolt [4]	5.55 (0.00)	-1.18 (0.84)	7.33 (0.14)	7.33 (-0.27)	2.72 (-0.37)	N/A	2.65 (0.00)	2.65 (0.75)
	MCC [9]	5.56 (-0.18)	-1.19 (0.00)	7.32 (0.27)	7.32 (-0.14)	2.73 (-0.74)	2.73 (1.44)	2.66 (-0.38)	2.66 (0.37)
	MCC [5]	5.57 (-0.36)	-1.17 (1.68)	7.29 (0.68)	7.34 (-0.41)	2.72 (-0.37)	2.74 (1.08)	2.65 (0.00)	2.64 (1.12)
$F = 0$ $a = 8 \times 10^{-3}$ $p = -1.0$	LoKI - MC	5.71 [0.04]	-2.59	7.34 [0.40]	7.55 [0.48]	2.81 [0.59]	2.91 [1.78]	2.75 [0.58]	2.63 [1.53]
	MultiBolt [4]	5.72 (-0.18)	-2.59 (0.00)	7.32 (0.27)	7.55 (0.00)	2.80 (0.36)	N/A	2.73 (0.73)	2.64 (-0.38)
	MCC [9]	5.73 (-0.35)	-2.60 (-0.39)	7.32 (0.27)	7.55 (0.00)	2.79 (0.71)	2.86 (1.72)	2.73 (0.73)	2.64 (-0.38)

Table 2: Comparison of the LoKI-MC solutions with the MultiBolt calculations [4] and previous MC results [5,9], for the Lucas-Saelee model. The LoKI-MC standard deviations  $\sigma[\%]$  and the errors  $\delta[\%]$  are calculated and presented as in table 1.

## 2 Real gases

For the benchmark in real gases, we use an ensemble of  $5 \times 10^4$  electrons and the simulations are stopped after  $10^5$  integration points. The gas temperature is 300 K and isotropic ionization scattering is considered. Additionally, we use the default values for the numbers of cells utilized to discretize the distribution functions and for the number of grid points to interpolate the cross sections, defined in [1].

For each gas, we compare the EEDFs and the swarm parameters calculated with LoKI-MC, LoKI-B (2-term solver) [2] and MultiBolt (10-term solver) [4]. The bulk diffusion coefficients from LoKI-MC are omitted for higher  $E/N$  due to significant fluctuations associated with the secondary electrons in ionization. These fluctuations can be diminished by increasing the number of electrons in the simulation, at expense of a higher computational time. We also provide the ratio of the lower-order anisotropies, averaged over all energies,  $\frac{\langle |f_{1,2}| \rangle}{\langle f_0 \rangle} \equiv \int_0^\infty |f_{1,2}(\epsilon)| d\epsilon / \int_0^\infty f_0(\epsilon) d\epsilon$ , calculated with LoKI-MC, in order to gain insight into the  $E/N$  regions where the two-term approximation might fail.

### 2.1 Ar

Cross-section set from IST-Lisbon database of LXCat [10].

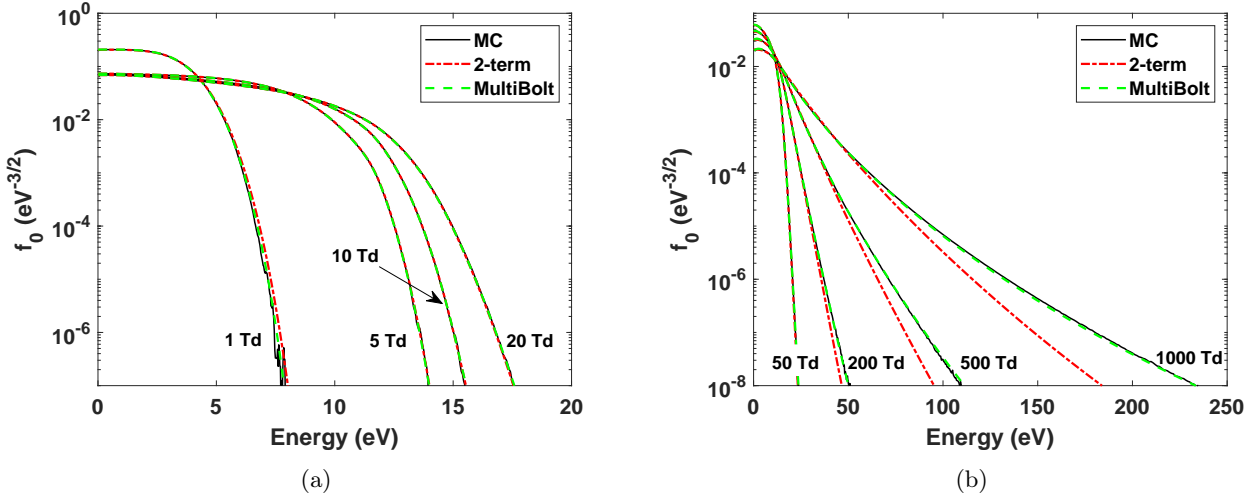


Figure 1: Electron energy distribution functions in argon, obtained with LoKI-MC, LoKI-B (2-term solver) and MultiBolt (10-term solver) for various reduced electric fields: (a) 1-20 Td; (b) 50-1000 Td.

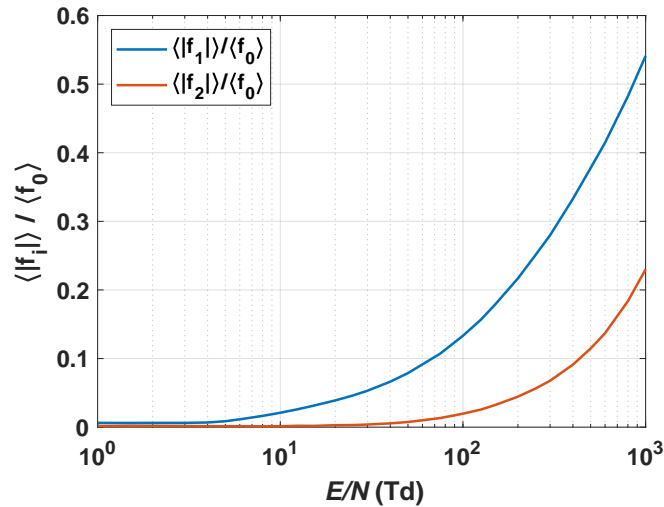


Figure 2: Average anisotropy ratios in argon, as a function of  $E/N$ :  $\frac{\langle |f_1| \rangle}{\langle f_0 \rangle}$  (blue);  $\frac{\langle |f_2| \rangle}{\langle f_0 \rangle}$  (orange).

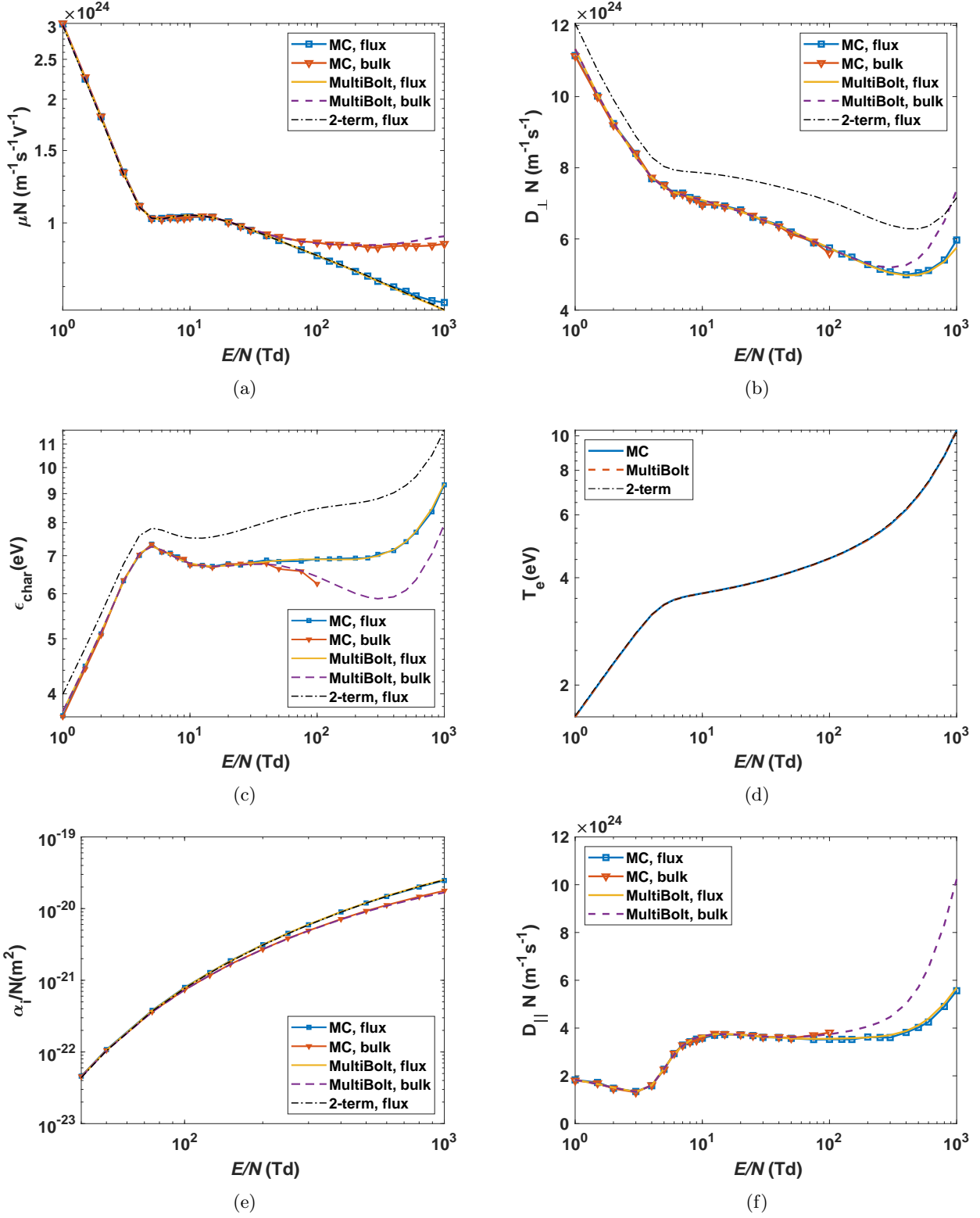


Figure 3: Electron swarm parameters in argon ( $T_g = 300$  K) as a function of  $E/N$ , obtained with LoKI-MC, LoKI-B (2-term solver) and MultiBolt (10-term solver): (a) reduced mobility; (b) reduced transverse diffusion coefficient; (c) characteristic energy; (d) temperature; (e) Townsend ionization coefficient; (f) reduced longitudinal diffusion coefficient.

## 2.2 CF<sub>4</sub>

Cross-section set from Hayashi database of LXCat [11].

**Important note on figure 6e:** the overestimation of the attachment coefficient calculated by MultiBolt, compared with LoKI-MC and LoKI-B, is caused by different approaches regarding the extrapolation of the cross section values for energies outside the range defined in the LXCat files. While LoKI-MC and LoKI-B set these values to zero, aiming to separate the data from the simulation tool, MultiBolt uses a mathematical expression for an extrapolation of these values.

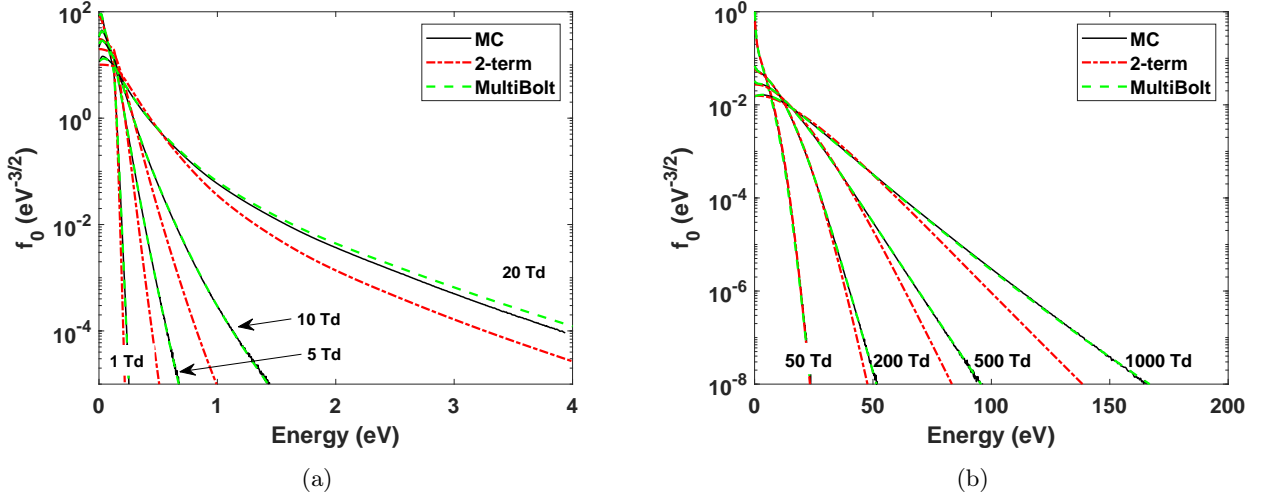


Figure 4: Electron energy distribution functions in CF<sub>4</sub>, obtained with LoKI-MC, LoKI-B (2-term solver) and MultiBolt (10-term solver) for various reduced electric fields: (a) 1-20 Td; (b) 50-1000 Td.

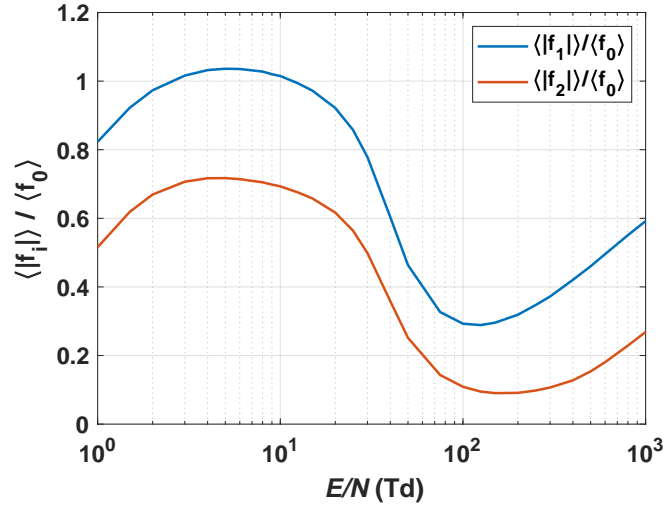


Figure 5: Average anisotropy ratios in CF<sub>4</sub>, as a function of  $E/N$ :  $\frac{\langle |f_1| \rangle}{\langle f_0 \rangle}$  (full lines);  $\frac{\langle |f_2| \rangle}{\langle f_0 \rangle}$  (dashed).

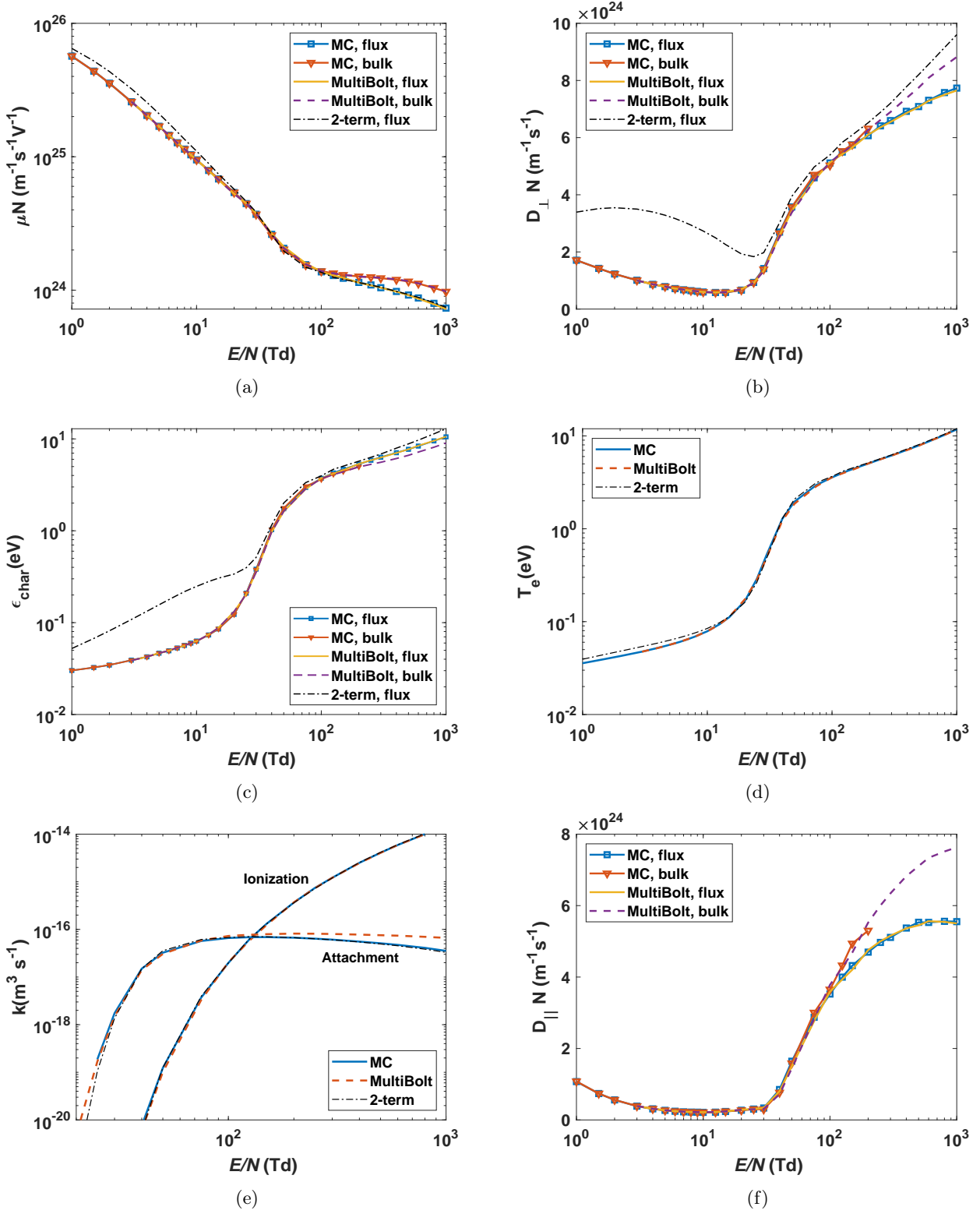


Figure 6: Electron swarm parameters in  $\text{CF}_4$  ( $T_g = 300$  K) as a function of  $E/N$ , obtained with LoKI-MC, LoKI-B (2-term solver) and MultiBolt (10-term solver): (a) reduced mobility; (b) reduced transverse diffusion coefficient; (c) characteristic energy; (d) temperature; (e) ionization and attachment rate-coefficients; (f) reduced longitudinal diffusion coefficient.

### 2.3 O<sub>2</sub>

Cross-section set from IST-Lisbon database of LXCat [12].

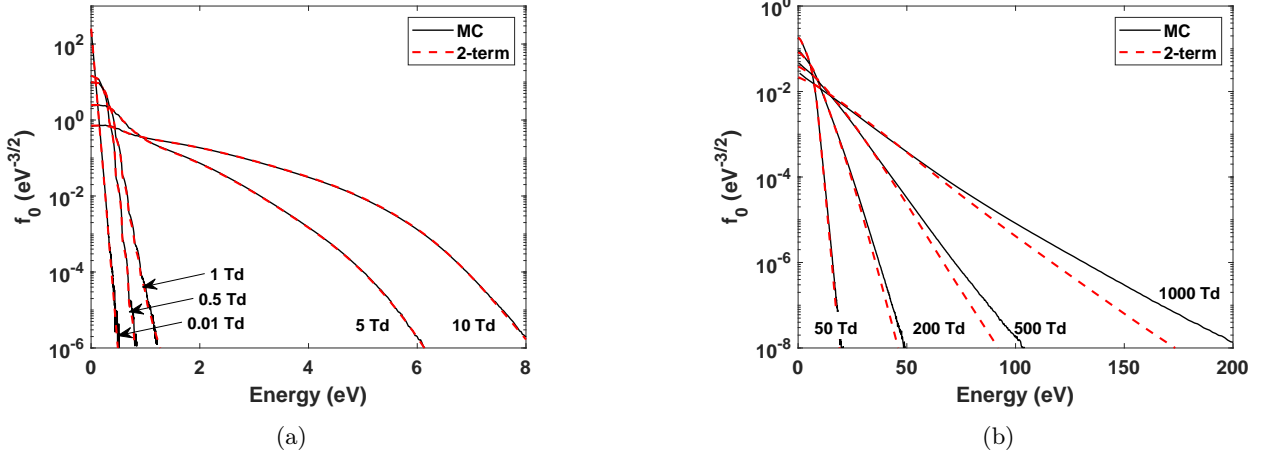


Figure 7: Electron energy distribution functions in oxygen obtained with LoKI-MC and LoKI-B (two-term solver), for various reduced electric fields: (a) 0.01 - 10 Td; (b) 50 - 1000 Td.

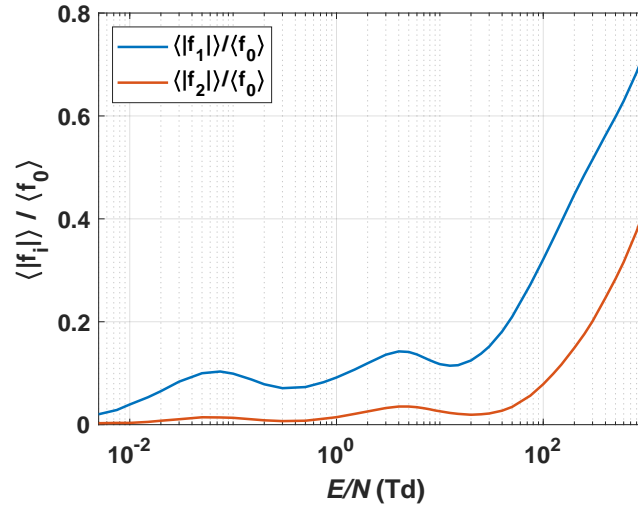


Figure 8: Average anisotropy ratios in O<sub>2</sub>, as a function of  $E/N$ :  $\frac{\langle |f_1| \rangle}{\langle f_0 \rangle}$  (full lines);  $\frac{\langle |f_2| \rangle}{\langle f_0 \rangle}$  (dashed).



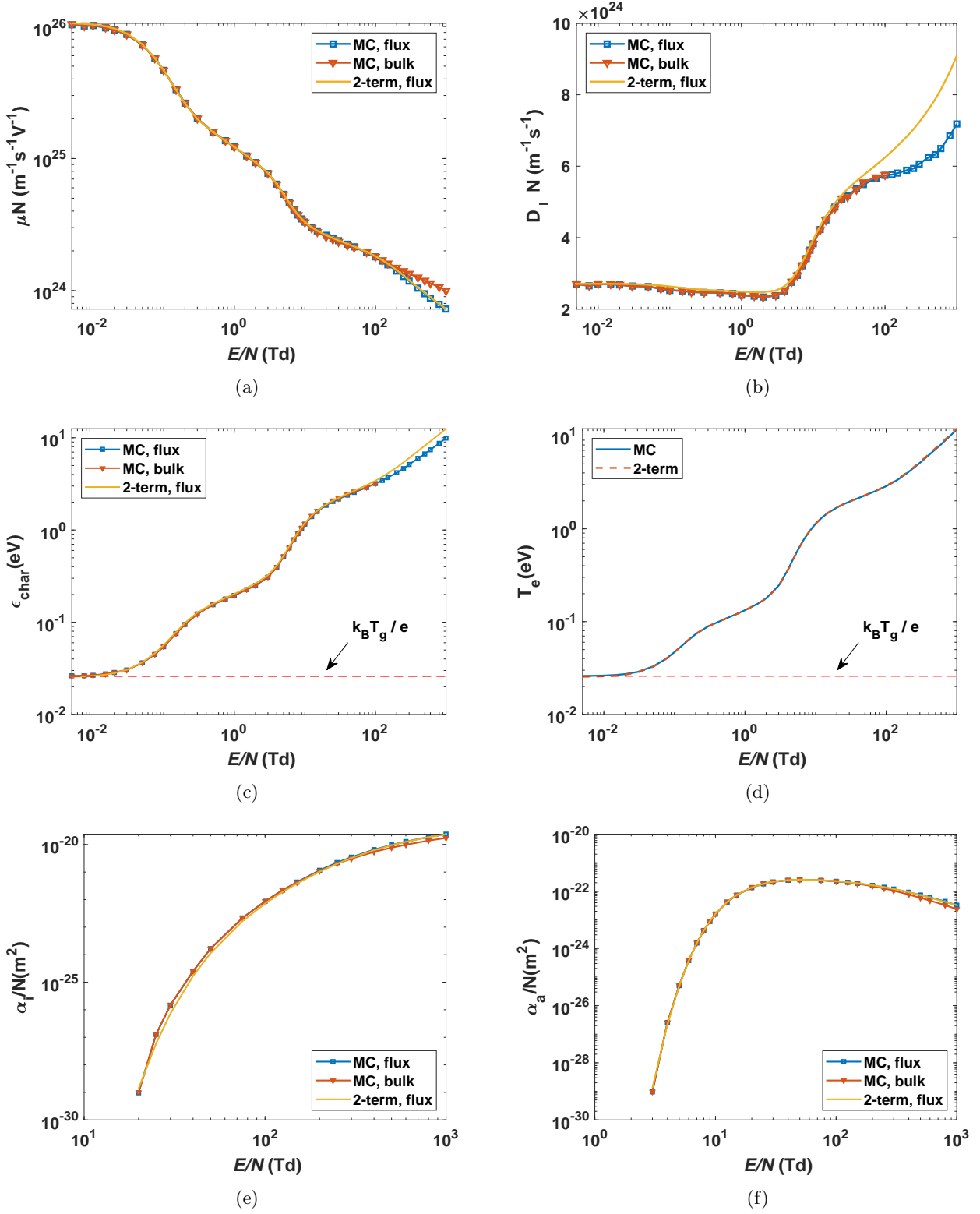


Figure 9: Electron swarm parameters in molecular oxygen ( $T_g = 300$  K) as a function of  $E/N$ , obtained with LoKI-MC and LoKI-B (2-term solver): (a) reduced mobility; (b) reduced transverse diffusion coefficient; (c) characteristic energy; (d) temperature; (e) Townsend ionization coefficient; (f) Townsend attachment coefficient.

## References

- [1] Dias T C, Tejero-del-Caz A, Alves L L and Guerra V 2022, *Comput. Phys. Commun.* 108554, doi: <https://doi.org/10.1016/j.cpc.2022.108554>
- [2] Tejero A, Guerra V, Gonçalves D, Lino da Silva M, Marques L, Pinhão N, Pintassilgo C D and Alves L L 2019 *Plasma Sources Sci. Technol.* **28** 043001
- [3] Reid I 1979 *Aust. J. Phys.* **32** 231
- [4] Stephens J 2018 *J. Phys. D Appl. Phys.* **51** 125203
- [5] Raspopovic Z, Sakadzic S, Bzenic S and Petrovic Z 1999 *IEEE Trans. Plasma Sci.* **27** 1241-1248
- [6] White R D, Brennan M J, Ness K F 1997 *J. Phys. D Appl. Phys.* **30** 810-816
- [7] Lucas J, Saelee H T 1975 *J. Phys. D Appl. Phys.* **8** 640-650
- [8] Ness K F and Robson R E 1986 *Phys. Rev. A* **34** 2185-2209
- [9] Nolan A M, Brennan M J, Ness K F and Wedding A B 1997 *J. Phys. D Appl. Phys.* **30** 2865-2871
- [10] Ar on IST-Lisbon database, [www.lxcat.net](http://www.lxcat.net)
- [11] CF<sub>4</sub> on Hayashi database, [www.lxcat.net](http://www.lxcat.net)
- [12] O<sub>2</sub> on IST-Lisbon database, [www.lxcat.net](http://www.lxcat.net)